Estonian Journal of Earth Sciences, 2022, **71**, 4, 214–229 https://doi.org/10.3176/earth.2021.15

Late Pleistocene to Middle Holocene record of sedimentation and carbonate content in the Zervynos paleolake-dune complex, Lithuania

Liudas Daumantas[a], Petras Šinkūnas[a*], Eugenija Rudnickaitė[a], Nikita Dobrotin[a], Dalia Kisielienė[b] and Andrej Spiridonov[a]

[a] Department of Geology and Mineralogy, Faculty of Chemistry and Geosciences, Vilnius University, M. K. Čiurlionio 21/27, 03101 Vilnius, Lithuania
[b] Institute of Geology and Geography, Nature Research Centre, Akademijos g. 2, 08412 Vilnius, Lithuania

*Corresponding author, petras.sinkunas@gf.vu.lt

Received 2 October 2022, accepted 23 November 2022, available online 1 December 2022

Abstract. The Late Pleistocene to the Holocene is a time interval that covers the climate transition from a cold to a warm interglacial regime. In the Baltic region, many studies have focused on estimating environmental responses to climatic forcing using palynological and stratigraphic proxies of glacial and periglacial settings. Herein we describe the mixed lacustrine-aeolian succession of the Zervynos-2 section (south-eastern Lithuania), located in the north-eastern part of the European Sand Belt. The succession and the sedimentation styles were characterized by granulometric parameters, structural features, dolomite/calcite ratio, and paleobotanical macro-remains. Our analyses revealed that the Zervynos-2 paleolake formed on the sandur (outwash) plain during the final stage of the Pleistocene. The onset of lake sedimentation was caused by sudden submergence of a sandbody-constrained paleovalley. Carbonate ratios and macro-remains from the lower gyttja material showed the presence of substantial millennial-scale oscillations, which suggests a delayed response to the isotopically derived paleotemperatures. The transition to the fast sand sedimentation started approximately in the Middle Holocene and is interpreted here as being caused by warming and drying of the climate in the Baltic region. The upper Holocene portion of the section represents the transition to exclusively aeolian sedimentation with lower accumulation rates that are likely related to a long-term cooling trend. The obtained results support the conjecture that there is a direct but delayed positive correlation between dolomite and calcite ratios in lake sediments and the climatic signal in the Greenland GISP2 record.

Keywords: European Sand Belt, sand, carbonates, plant macro-remains, climate events, Bayesian inference.

1. INTRODUCTION

The Late Pleistocene and the beginning of the Holocene were transformative time periods for biotic evolution, with increasing human influence on ecosystems (Koch and Barnosky 2006), changes in human-landscape interactions (Daumantas et al. 2020), and climatic modulation of human cultures (Donges et al. 2015). The end of the glacial period experienced some of the most extreme climate variations during the past one hundred thousand years (Broecker et al. 2010; Wolbach et al. 2018). Besides the general trend toward a warmer interglacial climate (Marcott et al. 2013; Veski et al. 2015; Stančikaitė et al. 2019), the millennial- and centennial-scale variability is detectable in global (Loehle and Singer 2010), North Atlantic (Bond et al. 1997), as well as south-eastern Baltic paleo-records (Spiridonov et al. 2019), which are studied here. The cold events, thought to be related to the disruption of oceanic circulation due to massive inputs of glacial freshwater (Keigwin et al. 1991; Teller et al. 2002; Ivanovic et al. 2017; Norris et al. 2021), are stratigraphically and climatologically important and widely correlatable episodes across the Baltic region (Veski et al. 2004; Stančikaitė et al. 2009; Druzhinina et al. 2020; Spiridonov et al. 2021).

Aeolian deposits present a unique and complex record of Late Quaternary environmental change in northern periglacial environments (Kasse 2002; Gaglioti et al. 2018) and cold mountainous deserts (Xu et al. 2018). Late Pleistocene to Holocene aeolian deposits could be a

precious source of information on the physical and biological change due to potentially very high sedimentation rates (thus high resolution) and relatively straightforward interpretation of granulometric data in terms of wind speeds and directions (Shao and Lu 2000), as well as occurrences of soil horizons, which are usually interpreted as representing periods of humid and/or decreased environmental energy (Clemmensen et al. 2001; Catuneanu 2006; White et al. 2013).

The European Sand Belt is a continental-scale and mostly periglacially determined geomorphological feature which stretches from France in the west to the north-western part of European Russia (Zeeberg 1998; Woronko et al. 2015). Recent works on sedimentological granulometry integrated with high-resolution stratigraphy revealed substantial insights into the prevalent climatic conditions during aeolian sedimentation of the sand belt, including unexpected episodes of extremely high wind speeds (Łapcik et al. 2021). Lithuanian late Quaternary aeolian deposits, which correspond to the north-eastern part of the European Sand Belt, show that the onset of the widespread wind-driven sedimentation started ~16 000–15 000 cal yr BP (Kalińska-Nartiša et al. 2015), and is interpreted to correspond to the end of the GS-2.1a cold episode (Rasmussen et al. 2014). Information on the development of the lake and river systems and the associated sand dune fields in the European Sand Belt during the Late Pleistocene, which is especially understudied for the Holocene (Tolksdorf and Kaiser 2012), reveals major environmental factors that enabled the recolonization of northern Europe by biota and associated development of human settlements (Daumantas et al. 2020). On the other hand, modern humans in various sandy environments of the Holocene, by means of fire use, animal husbandry, and forest clearing activity, should have acted as an essential feedback factor in aeolian geomorphodynamics (Lungershausen et al. 2018; Pierik et al. 2018).

The current study aims to describe and statistically test the paleo-environmental trends of the Late Pleistocene and Holocene as recorded in the mixed lacustrine-aeolian succession in the Zervynos paleolake-dune complex in south-eastern Lithuania (Fig. 1). The setting allows us to understand the temporal framework of qualitative sedimentation regime changes in the context of long-term climate evolution. To achieve this aim, this study integrated: (1) Bayesian construction of the age model based on the new stratigraphic analysis, IR-OSL dating of detrital material, and AMS ^{14}C dating of selected paleobotanical materials; (2) analysis of carbonate mineral composition and Monte Carlo Bayesian cross-correlational comparison of gyttja material from the lower part of the succession with the GISP2 ice core data; (3) sedimentological and carbonate geochemical characterization, and multivariate analysis of derived parameters of the upper sandy lacustrine-aeolian formation; (4) description of plant macro-remains found in the gyttja, and (5) interpretation of the derived patterns in the light of glacial-interglacial climate transitions in the Baltic region.

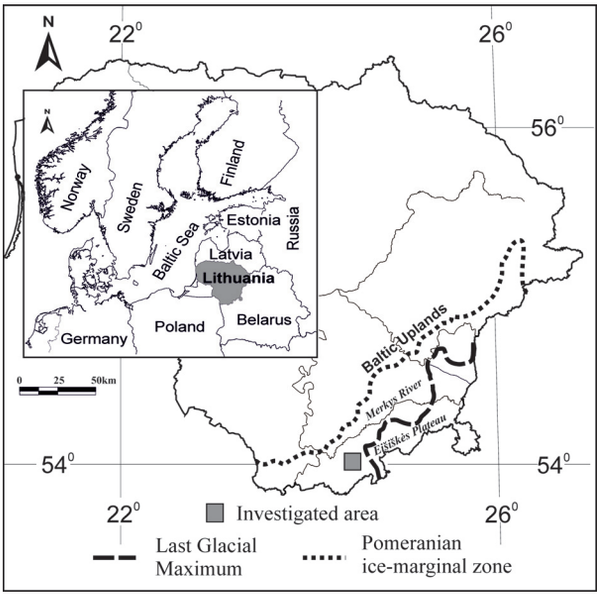

Fig. 1. Location of the study area. Glacial limits according to R. Guobytė (Guobytė and Satkūnas 2011).

2. PHYSICAL SETTING

The study area is located in south-eastern Lithuania in the vicinity of Zervynos village (Fig. 2). Glaciofluvial sediments of the distal outwash plain are the most widespread elements. In this distal position, the grain size of the outwash sediments is very suitable for aeolian transport, thus the dunes are widespread throughout the area. During the Last Glacial Maximum and the early stages of glacial retreat, braided meltwater streams formed an undulating outwash plain in front of a NE–SW trending belt of ice-marginal moraine ridges forming the Baltic Uplands. The system of glacial meltwater spillways running south-westward parallel to the ice-marginal morainic hills was embedded into the outwash plain surface close to its distal part during the Pomeranian stage of the last glaciation (Blažauskas et al. 2007). The present-day Merkys River (Fig. 1), flowing south-westward, followed this meltwater spillway system. To the south-east, the distal portion of the outwash meets the slopes of the Eišiškės Plateau formed during the Saale glaciation of the Middle Pleistocene. The distal part of the outwash plain and the

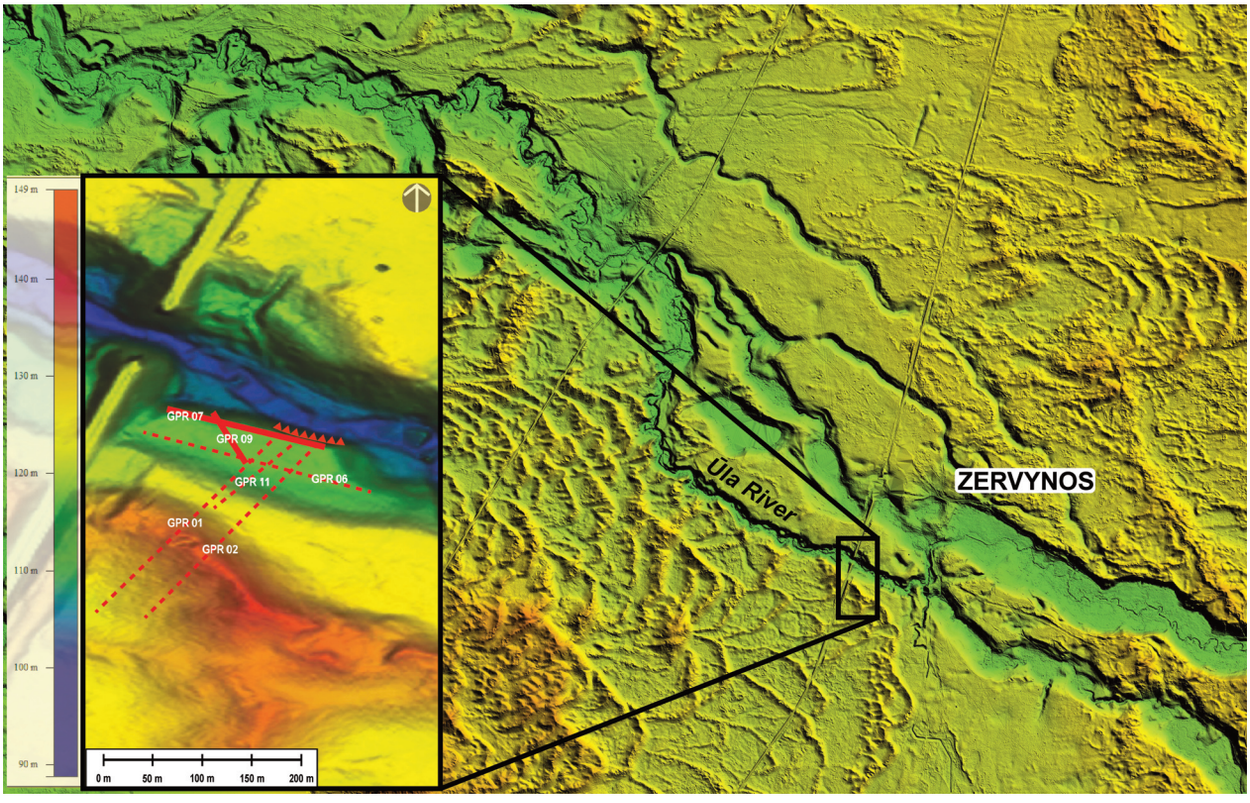

Fig. 2. Location map of georadar (GPR) profiles on the LiDAR DEM. Solid lines – GPR profiles shown in Fig. 4; dashed lines – other GPR profiles; sawtooth line – outcrop.

slopes of the plateau are now partly covered with aeolian sand.

Narrow dry valleys extend north-westward from the Eišiškės Plateau, reaching the glacial meltwater spillways that cross the outwash plain. The present-day course of the Ūla River is in the same direction. In addition, it follows the former tributaries of this valley system, switching from one paleovalley branch to another, deepening its valley until it joins the Merkys River. In places where the valley of the Ūla River (Fig. 2) crosses the older dry valleys, layers of lake sediments are exposed in outcrops on the left flank of the valley. One such outcrop is the newly found Zervynos-2 between Zervynos village and the railway bridge downstream, ~150 m upstream of the latter.

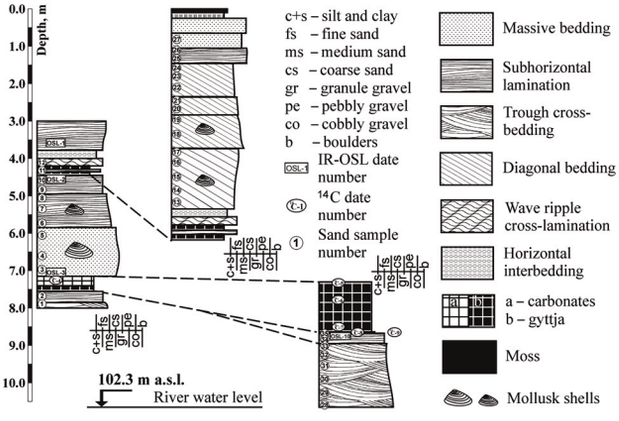

Fig. 3. Sediment succession of the Zervynos-2 outcrop profile. ^{14}C and OSL ages are presented in Table 3.

3. METHODS

3.1. Sampling and sedimentology

Thirty-five samples were taken from different points in the outcrop within sandy sediment layers (Fig. 3) for particle-size distribution analysis. The description of the sediment layers is provided in Table 1. The samples were taken at specific intervals to best reflect lithological variations. They were dry-sieved in the laboratory using a set of 19 sieves with a Fritsch rotap. The mesh size of the sieves was 0.0–2.50 mm. The material of the separated fractions was weighed to yield a weight precision nearest

Table 1. Description of the lithological characteristics of the Zervynos-2 outcrop

Depth, m	Lithology
0.00–0.25	Soil, black with humus, with a 10 cm cover of terrestrial moss on top.
0.25–1.45	Sand, greyish-white, various-grained with rare fine gravel, subhorizontally laminated, gradually shifting to massive yellowish light brown soil. The lower contact of the bed is abrupt.
1.45–2.84	Interbedding of fine and medium-grained sand, greyish-white, thicknesses of the diagonally inclined parallel laminas are 10–20 cm. The inclination of laminas is in the WSW direction at ~20 degrees. The layer thickens in the WNW direction.
2.84–3.78	Sand, greyish-white, fine-grained, thicknesses of the diagonally inclined parallel laminas are 2–10 cm, with concentrations of carbonate material particles along the lamina boundaries, with fragments of mollusk shells. Coarsening of sand, decrease of carbonate material, and thickening of the laminas are noticeable in the upper part of the bed. The inclination of laminas is in the WSW direction at ~20 degrees. The layer becomes thinner in the ESE direction.
3.78–4.00	Horizontally laminated interbedding of brown clayey silt and brownish-grey silty fine-grained sand. Thicknesses of the laminas are 0.5–2 cm.
4.00–4.20	Sand, yellowish-white, fine-grained, occasionally limonite-stained, indistinct wavy lamination characterized by higher contents of carbonate material. The contacts of the layer are gradational. The bed is inclined in the WSW direction at ~20 degrees.
4.20–4.45	Interbedding of light brown to black clayish gyttja with light yellow, fine-grained sand. The thickness of the interlayers is 4–10 cm. The bed is inclined in the WSW direction at ~20 degrees.
4.45–4.95	Sand, yellowish-grey in the upper part of the bed, yellowish-brown, slightly limonite-stained with increased carbonate content in the lower part of the bed, fine-grained, subhorizontally micro-laminated. The contacts of the layer are abrupt.
4.95–5.85	Sand, light yellowish-grey with brownish patches, medium-grained, subhorizontally and low angle cross-bedded, with mollusk shells.
5.85–7.15	Sand, light brownish-grey with yellowish patches, various-grained, predominantly coarse-grained, with gravel and mollusk shells and their fragments. The structure of sand is massive; the contacts of the layer are gradational.
7.15–7.30	Interbedding of light brown gyttja of low organic content and calcareous clay with an admixture of sand and silt, occasionally limonite-stained.
7.30–8.64	Gyttja, black. In the lowermost part of the layer has a ~1.5–5 cm thick layer of compressed terrestrial moss.
8.64–8.95	Sand, yellowish-grey, fine-grained, subhorizontally laminated, occasionally limonite-stained.
8.95–10.65	Sand, light grey, various-grained, predominantly fine-grained with scarce gravel and sporadic small pebbles, trough cross-bedded.

to 0.01 g. Data converted to weight per cent were used in all subsequent calculations.

3.2. Geophysical surveys

Six ground-penetrating radar GPR profiles ranging from 55.6 to 185.6 m in length were collected at the survey location (Fig. 2) using RADAR Systems GPR Zond 12-e, with a 300 MHz antenna, 400 V pulse generator and a time window (range) of 500 ns. Traces were collected at 5 cm intervals. A relative dielectric permittivity of 5.33 was calculated for the unsaturated dune sand, achieving ~30.0 m penetration at the maximum range. Elevations taken from LiDAR data were used to normalize the GPR images topographically.

All post-processing was performed with GVerse Geographix software. Two gyttja layers were traced from the outcrop near the river and interpreted in radargrams based on their strong signal returns and characteristic geometry. The coordinates of the GPR profile are presented in Table 2. The cross-sections GPR 07 and GPR 09 are shown in Fig. 4.

3.3. Carbonate analysis

Seventy-three samples were taken from the lower gyttja layer in the Zervynos-2 outcrop (Fig. 3) for carbonate composition analysis from a continuous volumetric column. The column was divided into 2-cm-thick intervals. Sub-

Table 2. GPR profile coordinates

Line ID	Start		End	
	Easting	Northing	Easting	Northing
GPR 01	24° 29' 10.7099"	54° 06' 20.6697"	24° 29' 16.6789"	54° 06' 26.4847"
GPR 02	24° 29' 12.3180"	54° 06' 20.4900"	24° 29' 17.9198"	54° 06' 26.1261"
GPR 06	24° 29' 19.7040"	54° 06' 24.6000"	24° 29' 12.2640"	54° 06' 26.5560"
GPR 07	24° 29' 18.1984"	54° 06' 26.0641"	24° 29' 13.0440"	54° 06' 27.3060"
GPR 09	24° 29' 15.6180"	54° 06' 25.5360"	24° 29' 14.5399"	54° 06' 27.1932"
GPR 11	24° 29' 14.5740"	54° 06' 24.0720"	24° 29' 17.3403"	54° 06' 26.3115"

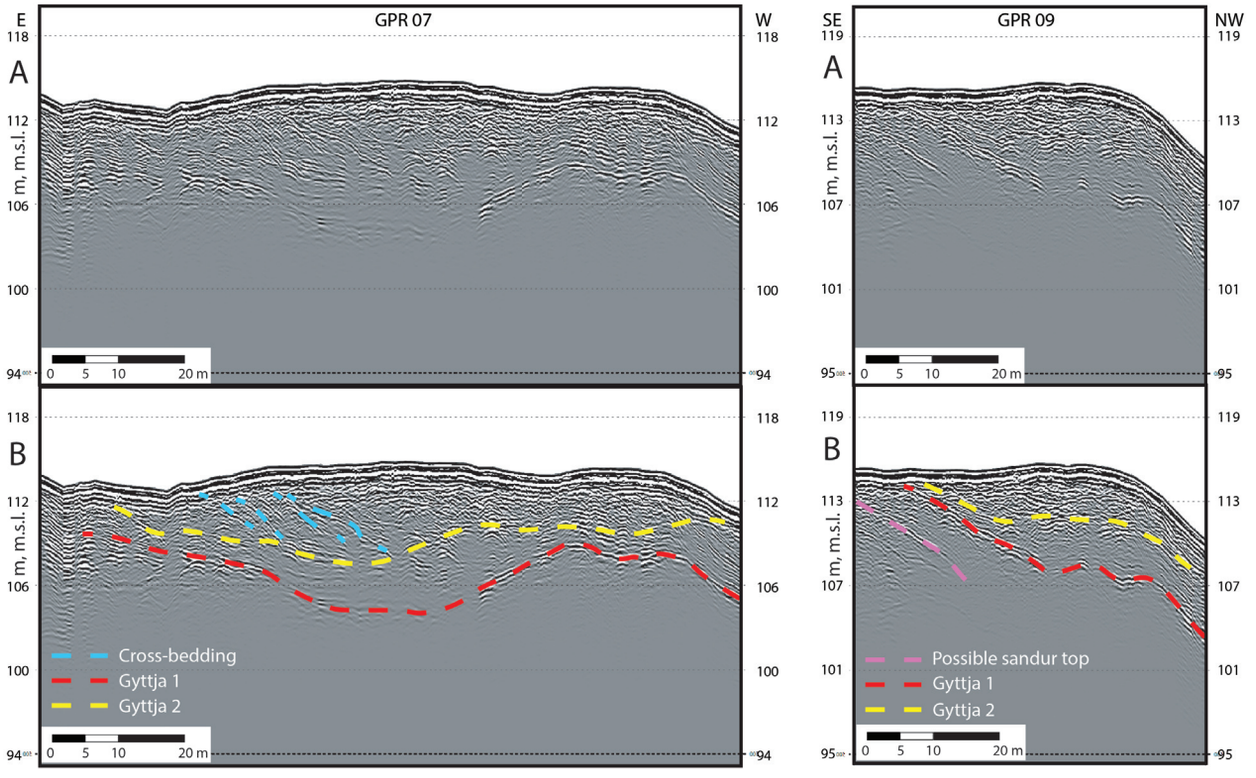

Fig. 4. Ground penetrating radar sections GPR 07 and GPR 09: A – raw/non-interpreted sections; B – with the interpreted location of the major lithological discontinuities, namely Gyttja 1 and Gyttja 2 layers, cross-bedding indicating progradation, and a possible sandur top or slope surface of the former valley.

samples were taken from each interval for the analysis of carbonates and plant macro-remains.

The carbonate analysis of bulk sediments was performed according to the improved method by Rudnickaitė (1980). A calcimeter was used to determine CO_2 volume. The same method was used to assess dolomite content. It is also possible to estimate other carbonate minerals if they are in significant amounts. The carbonate content in sediments was determined in the bulk sample. In order to calculate the mineral percentages, the volume of CO_2 related to calcite and dolomite was assessed at constant temperature during the reaction of these phases in HCl. The details of the carbonate analysis method have been described by Rudnickaitė (2007, 2016), Sanko et al. (2008), Kabailienė et al. (2009). The dolomite/calcite content ratio was later used as an implicit climate proxy

Table 3. Radiocarbon and OSL dates used in this study

No.	Dating method	Depth, cm	^{14}C Lab code	^{14}C age, yr BP	OSL/Calibrated ^{14}C age, cal yr BP	Dated material
1	OSL	358.0		–	5400 ± 400	Sand
2	OSL	455.0		–	6500 ± 400	Sand
3	OSL	705.0		–	7400 ± 500	Sand
4	^{14}C	725.0	Vs-3011	10 200 ± 90	11 884 ± 233	Carbonates
5	^{14}C	732.0	FTMC-FZ65-1	11 078 ± 49	12 994 ± 63	Plants/seeds
6	^{14}C	778.0	FTMC-FZ65-2	11 541 ± 49	13 404 ± 53	Plants/seeds
7	^{14}C	850.0	FTMC-FZ65-3	11 779 ± 49	13 641 ± 75	Plants/seeds
8	^{14}C	864.5	Vs-2994a	13 690 ± 195	16 569 ± 286	TOC
9	^{14}C	865.5	Vs-2994	13 900 ± 210	16 841 ± 304	TOC
10	OSL	875.0		–	56 000 ± 3800	Sand

and tested for statistical cross-correlations with the Greenland stable oxygen isotopic temperature record.

3.4. Plant macro-remain analysis

Seventy-three samples for plant macro-remain analysis were also taken from the lower layer of gyttja sediments (~150 cm thickness) enriched with organic matter. Each sample covered a 2 cm interval and had a volume of 500 mL. Plant macro-remains were extracted from the sediment samples by wet sieving (screens with a mesh size of 0.2 mm). The extracted organic matter was analyzed using a NICON SMZ 1500 microscope at a magnification of 20–60x. The discovered plant macro-remains were identified with the help of the atlases of Berggren (1969, 1981), Grigas (1986), Cappers et al. (2006) and a reference collection at the Nature Research Centre, Vilnius, Lithuania.

The TGView software (Grimm 2007) was applied to construct a diagram of plant macro-remains. Stratigraphically constrained cluster analysis (CONISS), a method of incremental sum-of-squares (without data transformation), was used to subdivide the paleobotanical diagram into local zones.

3.5. Dating and Age-Depth model

Six samples for ^{14}C dating were collected from an interval of 725.0–865.5 cm, at depths where appropriate quantities of dateable material were present. Additionally, four sand samples from other depths were used for optically stimulated luminesce (OSL) dating, extending the dated interval to 358–875 cm. The chronological information is provided in Table 3. ^{14}C samples Nos 5–7 were dated in the Mass Spectrometry Laboratory, Centre for Physical Sciences and Technology (FTMC), Vilnius, Lithuania. Accelerator mass spectroscopy (SSAMS, NEC, USA) and automated graphitization equipment AGE 3 (IonPlus AG) were used. Samples were treated by the acid/base/acid (ABA) method. The other ^{14}C samples (Nos 4, 8, 9) were taken later and analyzed by liquid scintillation spectrometry in the Laboratory of Nuclear Geophysics and Radioecology at the Nature Research Centre, Vilnius, Lithuania. The obtained ^{14}C dates were calibrated with the *Bchron* R package (Haslett and Parnell 2008) using the *IntCal20* calibration curve.

OSL dating was performed in the Research Laboratory for Quaternary Geochronology Department of Geology, Tallinn University of Technology, Tallinn, Estonia. Samples were collected in opaque containers to preserve the original signal of the last burial material after sunlight exposure. The potassium feldspar-based IR-OSL dating method was used for age determination (for details see, e.g., Molodkov and Bitinas 2006; Baltrūnas et al. 2010).

The Bacon Age-Depth (BAD) model was built for the 378.0–865.5 cm interval in R, using the *rbacon* package (Blaauw et al. 2021) in order to better understand the sedimentation history and to interpolate the ages of undated samples to allow for further chronologically meaningful statistical analysis. This depth interval has

nine dates, ranging from 5400 ± 400 OSL yr BP to 16 841 ± 304 cal yr BP. The oldest OSL date (56 000 OSL yr BP) was omitted from the model since it was taken from sediments below the depth range of interest and because of its outlying nature there were multiple competing explanations. The introduction of this date in the BAD model would have a negligible effect if a hiatus were modeled between it and the other dates. The used Bacon package *rbacon* applies Bayesian statistics approach to model the age-depth relationship, by combining date information with prior assumptions about the sedimentation processes to produce millions of possible deposition history scenarios. These scenarios are Markov Chain Monte Carlo (MCMC) iterations of deposition times (opposite of sedimentation rate, measured in yr/cm) assigned for an array of vertical sediment sections of a specified thickness. The zones of convergence of these different MCMC scenarios in the age-depth graph represent the most probable ages of the samples.

The depositional environments and sedimentation regimes inferred from the Zervynos-2 outcrop are pretty variable – there are seven depth levels where changes in sedimentation rate (SR) are expected. However, there are only nine dates suitable for age-depth model building, most of which fall between these inferred levels of SR changes. These conditions are very unfavorable for building traditional age-depth models that tend to locate changes in the SR at arbitrary points where samples for dating were collected. The errors produced in this way may confound the results of statistical analysis. However, the Bacon method package since version 2.3.2 (Blaauw 2018) has an argument *boundary* that allows to specify different prior sedimentation rates for different sections of the core. Also, it resets the autocorrelation of sedimentation rate, which allows abrupt sedimentation rate changes to be modeled where boundaries are placed. Thus, changes in sedimentation rate using *boundary* are more likely to align with structural, textural, lithological, or other boundaries specified in the model structure. In this paper, we would like to highlight and demonstrate the benefits of this *boundary* feature, as it is relatively new and potentially underappreciated.

The relevant BAD model input contains information about these boundaries, sedimentation rate priors and thickness (4 cm was used) of the vertical sections for which deposition times were modeled. The boundaries were placed at seven depths to separate eight different sedimentation regime units inferred from structural, textural, and compositional changes observed in the outcrop (Table 4). We have used the default "acc. shape" prior value of 1.5 for all identified units and only changed the "acc. mean" values according to the characteristics of each unit. To select "acc. mean" values, we have used the following protocol: (1) if an inferred sedimentation regime is "Typical lacustrine sedimentation", then select the average SR estimated from published dates or age-depth models of similar lakes present in the same region, if not, then (2) if there are at least two credible dates bounding or partly bounding the sequence, estimate the SR prior value from their ratio to depth, (3) if not, then find the most similar interval of deposits and if there are no signs that its SR was different, select it as an "acc. mean" prior value, otherwise, (4) slightly (< 30%) change it in the desired direction.

3.6. Statistical methods

3.6.1. Bayesian estimation of cross-correlation

In order to determine and test the statistical relationship between climate and carbonate sedimentation, which can exhibit a time lag, we performed a time series cross-correlation between the dolomite/calcite ratio and published paleotemperature data, which were modeled using stable isotope and ice accumulation data from the GISP2 ice core, central Greenland (Cuffey and Clow 1997; Alley 2000). The dolomite/calcite ratio was chosen here as a proxy for carbonate sedimentation since this variable combines the information of both dolomite and calcite percentages, as well as posits a positive correlation with paleotemperature, which might be easier to read visually in graphs than a negative correlation (if the opposite ratio of calcite/dolomite is used). Considering the climate proxy, GISP2 ice core data is a good, well-tested and popular proxy for global temperature changes (Easterbrook 2016).

In order to estimate the uncertainty of cross-correlation, we used 1000 different iterations of the BAD model (see the previous section for details) to assign dates to the carbonate samples. This process resulted in 1000 slightly different time series of dolomite/calcite ratios, which were then shifted in time using different lag values (from –2000 years to +2000 years). We linearly interpolated the values of paleotemperature and dolomite/calcite ratios at dates not represented in both datasets so that a sample-to-sample correlation between datasets would be possible. Finally, the Spearman correlation was measured at each lag between these alternative carbonate time series and the paleotemperature data for a corresponding time range. The Spearman rank correlation method was chosen as it is a more robust and symmetric measure of correlation in cases of ratio-transformed data and does not include assumptions about the linearity of the estimated relationship. Application of this method resulted in 1000 cross-correlation curves, all of which are possible according to BAD models. However, the concentrations of these curves and the average BAD model age curve present the highest likelihood scenarios for cross-correlation.

Table 4. Sedimentation regime units identified in the Zervynos-2 outcrop and the BAD model input related to these units

Interval identification	Depths of boundaries	Interpretation of sedimentation regime	Sedimentation rate prior, yr/cm	Rule used to select the prior
A	378 cm–TOP	Fast sedimentation, probable aeolian sand influx	3.6	3
B	445 cm–378 cm	Typical lacustrine sedimentation	14.8	1
C	495 cm–445 cm	Faster lacustrine sedimentation due to colder environment and erosion	10	4
D	715 cm–495 cm	Fast lacustrine sedimentation, terrigenous sand influx from slopes	3.6	2
E	730 cm–715 cm	Slow lacustrine sedimentation	136.2	2
F	850 cm–730 cm	Typical lacustrine sedimentation	14.8	1
G	864.3 cm–850 cm	Slow palustrine sedimentation in shallow water	136.8	2
H	BOTTOM–864.3 cm	Slow terrestrial sedimentation in a dry valley	210	2

3.6.2. Statistical analysis of granulometric patterns

Sedimentological parameters from the granulometric data were calculated using the GRADISTAT software (Blott and Pye 2001). As recommended by the software authors, the graphical Folk–Wald method was chosen as the statistical method because marginal fractions contained >1% and some >5% material. The Folk–Wald classification of parameter values was also chosen in the results section for sand samples from different paleo-environments. The metric scale was used instead of the phi scale to express grain sizes as this scale is more familiar to non-sedimentologists. Additionally, the Trask coefficient was calculated using the Tucker formula as a square root of P75/P25, with percentiles in phi units (Conwy Valley Systems Limited 2022).

Several depositional environments were distinguished based on textural-structural differences and field inspections. We used the *Random Forest* application in R (Liaw and Wiener 2002) to estimate how well each sedimentological parameter defines the established paleo-environments. The Random Forest is a machine learning method that uses subsamples of data to build many Classification and Regression Tree (CART) models with random elements. In this study, each such CART divided the data by the values of sedimentological parameters in such a way that it provided the purest (as measured by reductions in Gini index values) classification in the given depositional environments. Sedimentological parameters that, on average, produced the highest reductions in the Gini index were considered the best parameters to discriminate between depositional paleo-environments.

4. RESULTS

4.1. Age model

The produced BAD model exhibits a step-like shape and punctuated changes in sedimentation rate at the specified boundaries between structurally, texturally, and com-

positionally different units of the Zervynos-2 outcrop (Fig. 5). The highest sedimentation rates were modeled in units A and D, where gravitational flows and the influx of terrigenous sand were suspected; the medium SR in units B, C and F of "typical/fast lacustrine sedimentation"; the lowest SR in units E, G and H, where slow sedimentation or even no deposition was expected. Thus, five abrupt SR changes occur at the interfaces of units G–F, F–E, E–D, D–C, and B–A (D–C change being the least abrupt), and two less prominent SR changes occur between units G–H and B–C. Also, there are visible variations in levels of uncertainty. In the uppermost part of the outcrop, they are inflated by broader distributions of OSL dates and a smaller number of dates per depth. In the lowermost part, 95% confidence intervals are wider but narrower upward in unit F, probably due to the uncertainty in SR caused by the older, less constrained 8–9 dates (Table 3). However, most of the probability mass is still concentrated in a relatively small area (darker area in unit F, Fig. 5), indicating that higher SRs are more likely in unit F. Thus, the produced BAD model shows a substantial variation of the SR correlated with the specified boundaries of structural, textural and compositional changes.

4.2. Statistical cross-correlations between carbonates and GISP2 record of Greenland temperatures

Visual inspection of the temperature and dolomite/calcite ratio time series hints at a possible delay of the dolomite/calcite ratio response to climate change since both time series have a similar shape. However, peaks and troughs of the curves are not aligned (Fig. 6A). Indeed, the results of the Bayesian cross-correlation analysis between these time series reveal that a much stronger correlation exists at non-zero time lags (Fig. 6B). However, the correlation of the original time series (at a zero time lag), even though less likely, can also be similarly strong (16–84% confidence intervals (CI) are 0.01–0.48). This can be visually observed in the overlap between the age uncertainty bars of peaking dolomite/calcite ratio samples and the temperature peaks (Fig. 6A).

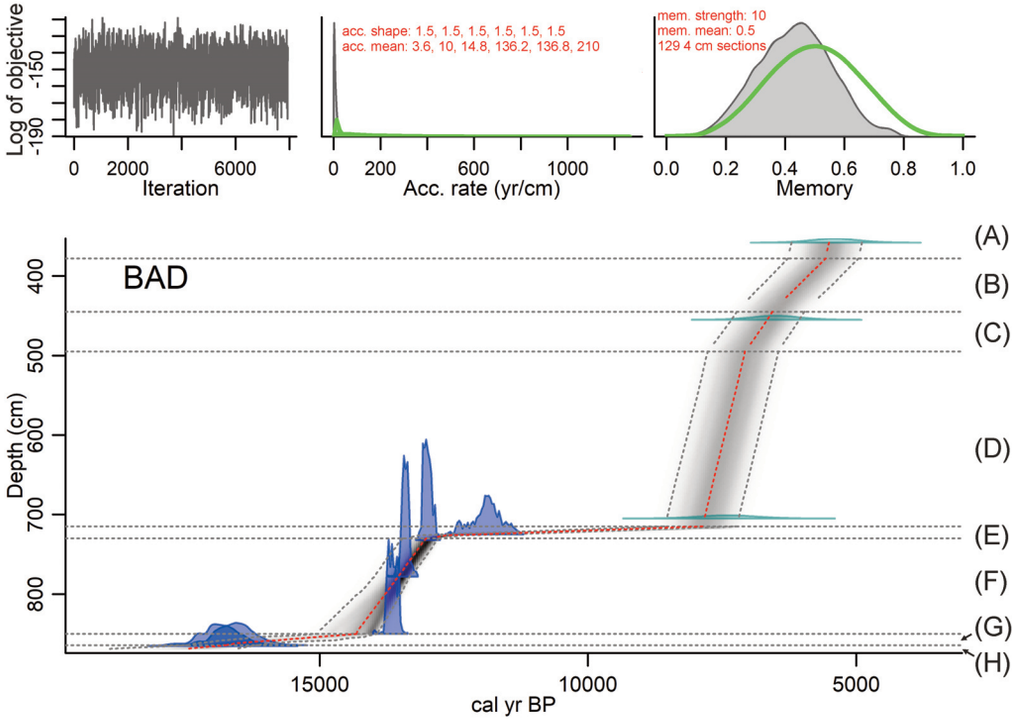

Fig. 5. Graphical output of the BAD model of the Zervynos-2 outcrop. The upper left graph shows the performance of the MCMC iterations (general randomness, stationarity and no structure are all signs of good models). The top middle graph demonstrates the characteristics of the prior (green) and posterior (grey) distributions of the accumulation rate, whereas the upper right graph represents the distributions of memory (autocorrelation of sedimentation rate). Written in red are the parameters of the prior distributions used, as well as the "thick argument" value with the resultant number of sections. The lower graph depicts the calibrated radiocarbon dates (blue) and OSL dates (greenish blue) as well as the age-depth model. The darker color highlights the more probable calendar ages, whereas the 95% confidence intervals are presented by dashed lines. The red line connects the mean ages of each sample and presents the mean BAD model. The capital letters on the right refer to the distinguished sedimentation regimes in Table 4, whereas the horizontal dashed lines indicate their boundaries.

Nevertheless, more probable and higher positive correlations are observed at lags between 300 and 1500 years. In contrast, most of the highest correlations occur at lags between 340 and 700 years (e.g. 18–82% PI at 640 SR lag is 0.34–0.66). Also, the prominent moderate negative correlations are concentrated at negative lags between –1500 and –500 yrs. Most of the lowest correlations occur between lags of –1460 and –980 years (e.g. 18–82% PI at –1080 yrs lag is from –0.54 to –0.28). Thus, these results support the conjecture that there is a direct but delayed positive relationship between dolomite and calcite ratios in gyttja and the climatic signal (as reflected by temperature) in the Greenland GISP2 record.

4.3. Stratigraphic distribution of plant macro-remains

The stratigraphically constrained cluster analysis revealed the presence of seven plant macro-remain assemblage zones (Fig. 7). Here, the zones are listed from the deepest (oldest) in the gyttja to the shallowest (youngest). The depth intervals are calculated from the top of the outcrop.

The oldest zone Zm-1a corresponds to a depth interval of 855–875 cm. Based on the Bayesian age model, its lower part could be as old as almost 17 000 cal yr BP, whereas the upper part is closer to 13 500 cal yr BP. Thus, it corresponds to the longest part of the gyttja record and is the longest macro-remain assemblage zone analyzed here. In it, aquatic plants (*Chara* sp., *Potamogeton alpinus*, *P. filiformis*, *P. vaginatus*) dominate the record; *Carex*, which grows on wet shores, is widespread; especially abundant are green moss and pine in the vicinity of the basin.

The second oldest zone Zm-1b corresponds to a depth interval of 821–855 cm. The macro-remains are dominated by birch (*Betula*) and pine (*Pinus*). Water and wetland plant residues are substantially reduced. The dominant species in the latter plant group do not change.

The third zone Zm-2 corresponds to a depth interval of 801–821 cm. There is a substantial reduction in plant macro-remains. Among them, the most abundant is *Betula* sect. *Albae*. The remains of *Schoenoplectus lakustris* and *Menyanthes trifoliata*, characteristic of marshy shores of the water basin, are also found in the record.

The fourth zone Zm-3 corresponds to a depth interval of 789–801 cm. The plant macro-remains are scarce. Birch and pine predominate in the terrestrial vegetation of the area, the most dominant forms are *Hippuris vulgaris* in the water body and *S. lacustris* in the coastal community.

The fifth zone Zm-4 corresponds to a depth interval of 769–789 cm. Here the number of plant macro-remains and the diversity of species increases. Deciduous trees are represented by *Betula* sect. *Albae*, *B. nana* and *Alnus* sp., conifers by *Larix* sp. and *Pinus* sp. The latter species dominates among the trees. Among the aquatic plants, *P. filiformis* is slightly more abundant, and *Carex* species are widespread along the coast.

The sixth zone Zm-5 corresponds to a depth interval of 757–769 cm. The abundance of plant macro-remains is

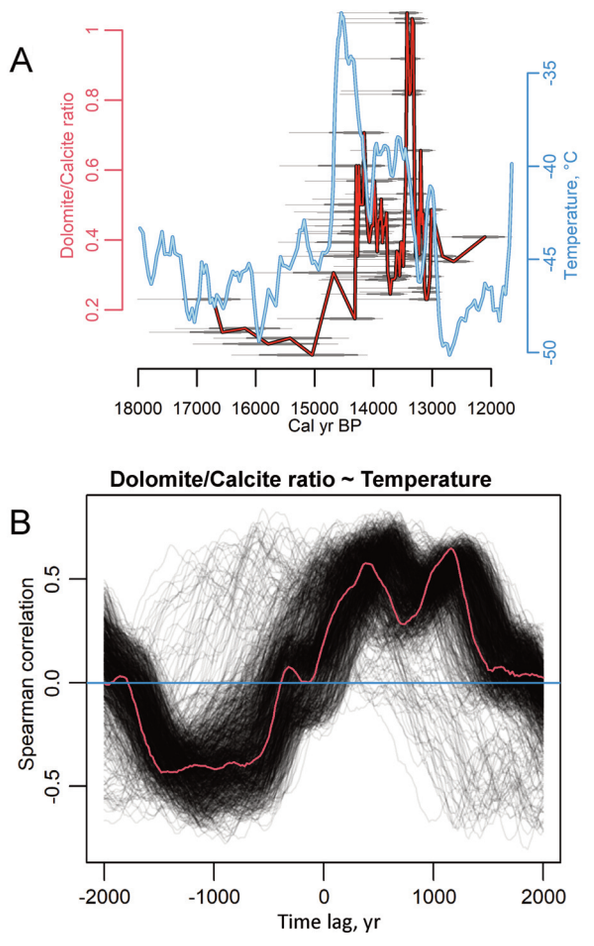

Fig. 6. Analysis of statistical correlations between dolomite/calcite ratios in the Zervynos-2 lower gyttja section, and GISP2 temperature data: A – time series of dolomite/calcite ratio (red) and GISP2 temperature (light blue). The red line represents the average dolomite/calcite ratio time series, whose samples were assigned the average dates from the BAD model posterior distributions. The horizontal bars depict the probability intervals (PI) of the date of each sample (narrow bars: 2–98% PI, medium bars: 6–94% PI, wide bars: 16–84% PI). B – curves of cross-correlation between dolomite/calcite ratio and GISP2 temperature. Each black curve represents a different iteration of the BAD model, and the red curve – the mean BAD model. The horizontal blue line separates positive and negative correlations. Positive time lag values mean that the carbonate time series were shifted back in time and vice versa. A high correlation at positive lag values shows the delayed response of carbonate compositions to climate change, as measured in GISP2.

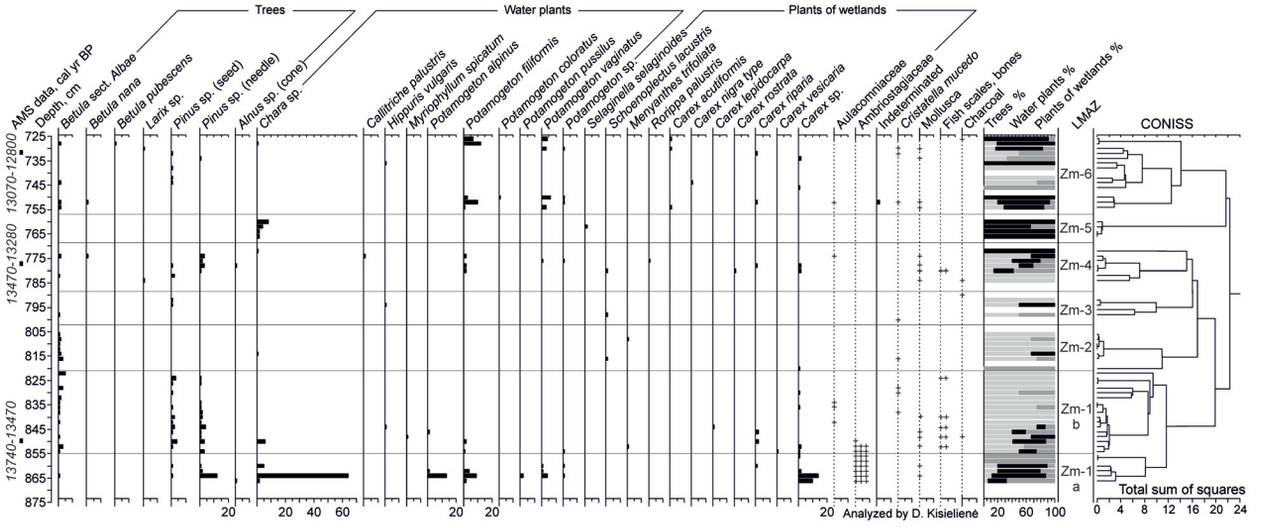

Fig. 7. Stratigraphic distribution of plant macro-remains. Assemblage zones were determined using stratigraphically constrained cluster analysis. Depth is given in cm from the top of the outcrop. The zones are listed from the oldest to the youngest (Zm-1a to Zm-6).

low. *Chara* sp. dominates in the water body, *Selaginella selaginoides* is prevalent along the coast.

The seventh and youngest zone Zm-6 corresponds to a depth interval of 725–757 cm. Based on the integrated age model described above, this zone probably corresponds to a time interval from > ~13 100 and up to possibly 12 100 cal yr BP. The abundance of plant macro-remains here is higher than in the previous zone Zm-5. The variety of trees is increasing and reaches a similar diversity as in zone Zm-4. The water basin is dominated by *P. filiformis* and *P. vaginatus*, whereas various species of *Carex* predominate along the coast.

4.4. Granulometric trends

The ability to distinguish between depositional environments identified based on the Random Forest modeling of the analyzed granulometric variables is presented in Fig. 8. The uncorrelated sedimentological variables are shown in Fig. 9. Based on Fig. 8, it appears that grain size parameters (except for a mode) are better descriptors of the depositional environments, with median size marginally leading. It is even clear from Fig. 9 that median grain size is a better descriptor since the fluctuation in the values of this parameter is more pronounced where changes in the depositional environment occur (Fig. 9). However, due to the overlapping ranges of grain sizes, more than this parameter is needed to differentiate the paleo-environments. Nevertheless, these paleo-environments are represented by relatively different skewness and sorting of sand and can therefore be discriminated in crossplots of these parameters versus grain size.

The sediments in the lowermost part of the outcrop interpreted as "sandur" deposits are mostly moderately well-sorted medium sands, characterized by kurtosis varying from very leptokurtic to mesokurtic, and skewness from fine-skewed to very coarse skewed.

The "valley bottom" sediments formed before the deposition of gyttja are well-sorted and moderately well-sorted, with coarse median grain size (~700 μm), symmetric distribution and mesokurtic kurtosis.

The "gravitation input" sand deposits consist of relatively finer (~250–350 μm), moderately well-sorted, leptokurtic-mesokurtic medium sands characterized by a general trend of increasing sorting toward the top of the section and skewness changing from fine-skewed (–0.26) to symmetric (0.02). According to the BAD model, sedimentation of these deposits started at ~7800 cal yr BP and ended at ~6700 cal yr BP.

Sedimentation of "shallow lake" deposits was initiated after that, lasting for around ~1500–2000 years. "Shallow lake" deposits are mainly well-sorted, characterized by coarse grains (550–700 μm), symmetric distribution and platykurtic-mesokurtic kurtosis.

The upper part of the section interpreted as "lake sediments with aeolian input" is occupied primarily by well-sorted medium sands (~350–450 μm), with skewness varying from fine-skewed to coarse-skewed and kurtosis from leptokurtic to mesokurtic.

4.5. Geophysical surveys

The GPR 07 cross-section was measured along the outcrop; therefore, the reflection surfaces Gyttja 1 and

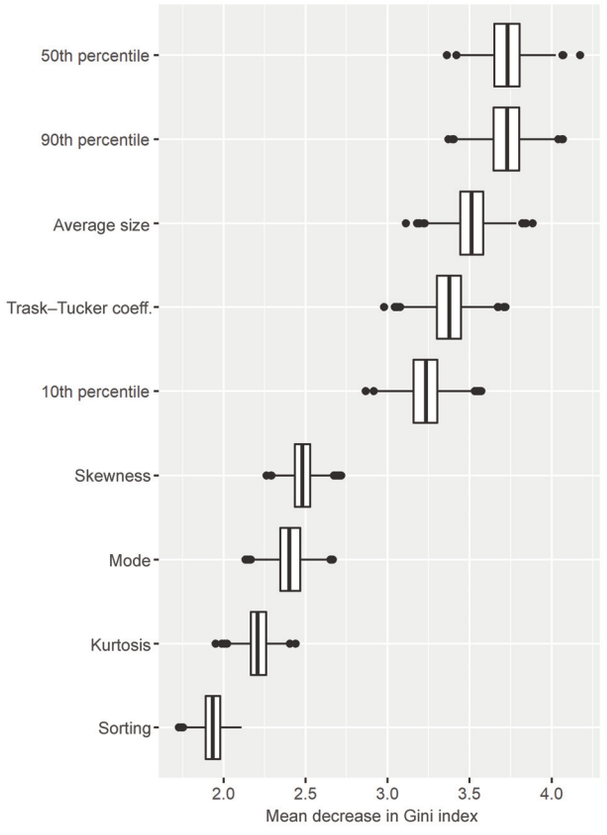

Fig. 8. Importance of granulometric parameters in distinguishing between the identified depositional environments, as evaluated by Random Forest variable importance estimation. The larger the magnitude of the decrease in the Gini index by a variable, the more powerful it is in recognizing different depositional environments.

Gyttja 2 were easy to identify (Fig. 4). In the eastern part of the GPR 07 cross-section, the surface of Gyttja 2 nearly reaches the ground surface. The cross-bedding seen in the outcrop (Fig. 3) can also be traced in the GPR data (light blue dashed line in Fig. 4B). The geological interpretation of the GPR 09 line is also presented in Fig. 4B. Similarly, Gyttja 1 and Gyttja 2 surfaces are visible in the radargrams. In the south-eastern part of the GPR 09 cross-section, Gyttja 1 and Gyttja 2 surfaces nearly reach the ground surface. In addition, one more unidentified surface is visible in the GPR data (pink dashed line). Due to the surface location and geometry, it can be interpreted as a possible sandur top or slope surface of the former valley.

5. DISCUSSION

The sedimentary succession of the Zervynos-2 outcrop, based on a range of sedimentological, geochemical and paleobotanical evidence, represents a transition between the proglacial sandur environments of the Late Pleistocene through a lake stage (from the latest Pleistocene to the Early Holocene 16 000 to 8000 cal yr BP), which finally transitioned to the environment dominated by aeolian processes in the Middle to Late Holocene (<8000 cal yr BP). Since the succession has been formed in qualitatively very different environments, we focused here more on the period from the end-glacial to the Holocene, which documented the critical climatic transition to a modern warm state.

The onset of the formation of the Zervynos-2 paleolake was most probably related to the interaction of local geomorphic factors, which allowed sudden damming of the area, which can be inferred by an exceptional preservation of the terrestrial moss, above which typical lake sediments started to form. The gyttja, which formed in the earliest stages of lake development, shows a record of relatively calm and anoxic bottom environments, which allowed the accurate dating of sediments, as well as their paleobotanical and carbonate geochemical characterization. Seven paleobotanical assemblage zones distinguished in gyttja show that substantial changes in plant taxonomic composition happened approximately every millennium or around that time. This millennial-scale climatic variability is also confirmed by the carbonate compositional record and its cross-correlation with the GISP2 temperature record. An interesting fact is that there is a substantial lag, given all age uncertainties, from 600 to 1200 years between the dolomite/calcite ratio and the Greenland paleotemperatures. There could be at least two explanations for this pattern: (1) there is a regional delay in the climate response in central Europe in comparison to Greenland (this was recorded in other studies, which are based on pollen records from bogs of the same region of southern Lithuania (Spiridonov et al. 2019; Stančikaitė et al. 2019) and (2) the lag is out of phase with the increasing temperature solubility of calcite and dolomite, which can be related to other variables that covary with temperature – for example, a delayed increase in humidity as a function of rising temperatures can cause such a delayed response. The differentiation of these alternatives requires systematic comparisons of paleotemperature records with dolomite/calcite time series from various regions.

The dominant millennial-scale climatic variability, which is detectable in the lower part of the Zervynos-2 section with both Bølling and Allerød, is apparent in the dolomite/calcite ratios with substantial time delays in comparison to the GISP2 temperature record. These millennial-scale oscillations are close in their duration to the so-called Bond events detectable in the Late Pleistocene and Holocene paleoclimate proxies (Bond et al. 1997; Bond et al. 2001). The millennial to multi-

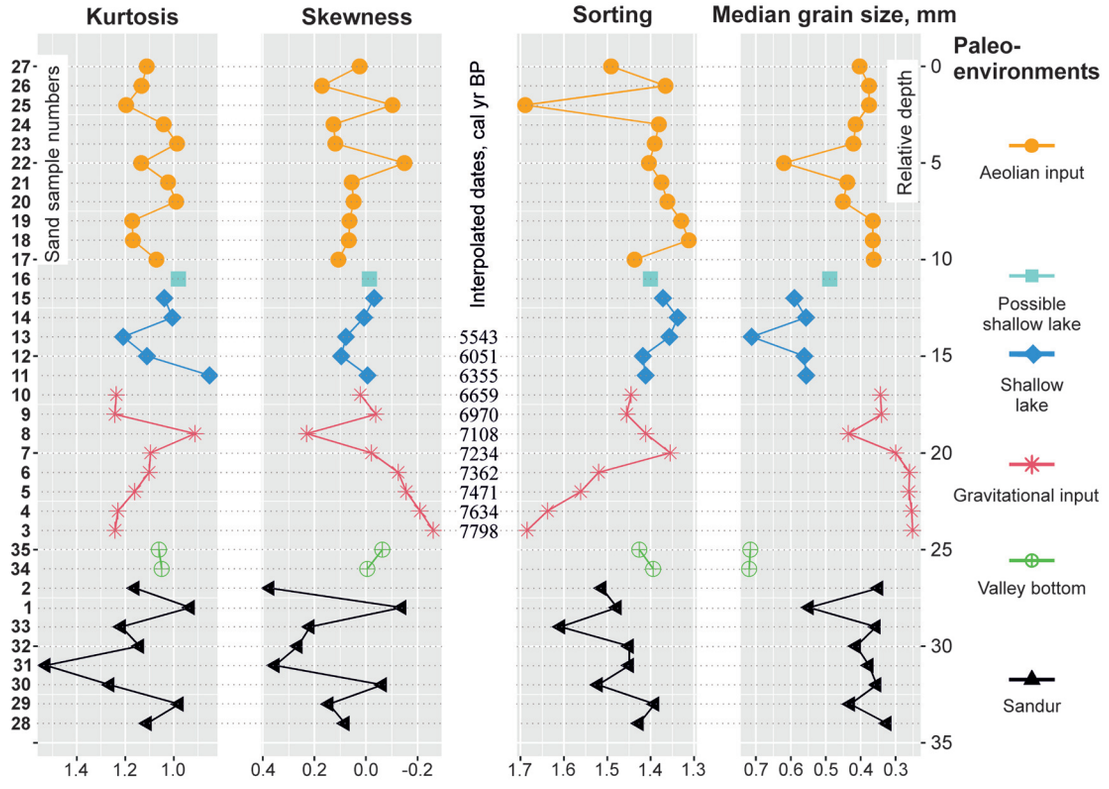

Fig. 9. Values of uncorrelated sedimentological parameters along the outcrop with interpreted depositional paleo-environments. Since all grain size parameters and the Trask coefficient constituted a group of correlated variables, only the median grain size was chosen for display, as it is a marginally better descriptor of the identified depositional environments (Fig. 8). The age dates are estimated using the Bacon age-depth model that was trained on both radiocarbon and OSL dates.

millennial-scale periodic variability, detected in the Late Pleistocene and Holocene paleobotanical records of Lithuania, has previously been linked to non-linear higher frequency responses of the ocean system to the Milankovitch forcing (Spiridonov et al. 2019).

The thick lower gyttja layer, which formed during a period of approximately five thousand years, transitioned around the beginning of the Holocene (~12 000 cal yr BP) to slow sandy sedimentation. After approximately 8000 cal yr BP, the sedimentation rates increased dramatically and the dominant sediments became lacustrine sands. The Zervynos-2 paleolake is located in a paleodune field (Fig. 2), therefore a possible driver of sedimentation change could have been the intensification of sand transport by means of aeolian processes and hill slope erosion, which must have been caused by the onset of a warmer climate during the intense deglaciation of the Northern Hemisphere. As tree biomass increased in boreal environments at the onset of the Holocene, and average temperature increased simultaneously, this likely produced an environment conducive to more frequent wildfires, which enabled more intensive erosion (Matthews and Seppälä 2014). The Middle Holocene (Northgrippian Age) was the warmest time interval of the epoch in the Baltic region (Borzenkova et al. 2015; Spiridonov et al. 2019). During the Holocene Thermal Maximum, most of northern Europe was characterized by a warm and dry climate (Snowball et al. 2004; Stančikaitė et al. 2019). Therefore, this time interval was very conducive to frequent forest fires, which were probably in no small part caused by humans (Pierik et al. 2018), and which dramatically increased in abundance throughout the Holocene.

The upper part of the Zervynos-2 section is composed of sands likely with substantial aeolian input. Their age is not well constrained, but the maximum age, based on the Bayesian model, should be less than 5500 cal yr BP (Fig. 9). Most probably, the lacustrine-aeolian transition occurred as a consequence of normal regression – the depletion of the sediment accommodation space in the paleolake (Miall 2010), which occurred at the end of the Northgrippian Age. The succession of purely aeolian sands, which in the uppermost part are massive (thus bioturbated), shows that aeolian activity and landscape change continued in the latest part (Meghalayan) of the

Holocene. It has been shown earlier that in Lithuania, during the regional Subboreal age (early Meghalayan), there was a decrease in aeolian activity (Molodkov and Bitinas 2006). The relatively thin aeolian section of the succession in the Zervynos-2 outcrop (<2 m) shows a limited opportunity for accumulation of the transported sand during the latest part of the Holocene, which confirms earlier assertions about a reduction in aeolian activity.

CONCLUSIONS

The study of the Zervynos-2 outcrop, located in south-eastern Lithuania, revealed that:

1. The formation of the Zervynos-2 paleolake in periglacial environments was a sudden process related to submergence of the valley, most probably related to the drift of dunes and other sand bodies across an outwash (sandur) depocenter during the Late Pleistocene.
2. The first stage of the development of the Zervynos-2 paleolake was characterized by slow sedimentation of organics and carbonate-rich gyttja, which terminated at the beginning of the Holocene.
3. The paleobotanical and dolomite/calcite ratio analysis of gyttja revealed that the Late Pleistocene environments experienced substantial millennial-scale climatic fluctuations. Interestingly, however, the response of carbonate mineral ratios was delayed by several hundred to a thousand years in comparison to the temperature fluctuations in Greenland.
4. The increase in sedimentation rates in the Zervynos-2 paleolake and its subsequent transition to a terrestrial regime was coincident with the transition to the Holocene and the emergence of warmer and drier climate conditions enabling the increase in aeolian transport and hillslope erosion, which served as the major source of sediments during the past 8000 cal yr BP.

Acknowledgements. The authors were supported by the Research Council of Lithuania grant (S-LL-18-2). We thank Miglė Paškevičiūtė for the sediment grain-size analysis. The reviewers Ilya V. Buynevich and Siim Veski are acknowledged for their constructive remarks. The publication costs of this article were covered by the Estonian Academy of Sciences.

REFERENCES

Alley, R. B. 2000. The Younger Dryas cold interval as viewed from central Greenland. *Quaternary Science Reviews*, **19**(1–5), 213–226.

Baltrūnas, V., Karmaza, B., Molodkov, A., Šinkūnas, P., Švedas, K. and Zinkutė, R. 2010. Structure, formation and geochronology of the late Pleistocene and Holocene cover deposits in South-Eastern Lithuania. *Sedimentary Geology*, **231**(3–4), 85–97.

Berggren, G. 1969. *Atlas of Seeds and Small Fruits of Northwest-European Plant Species with Morphological Descriptions. Part 2, Cyperaceae*. Berlingska Boktryckeriet, Lund.

Berggren, G. 1981. *Atlas of Seeds and Small Fruits of Northwest-European Plant Species with Morphological Descriptions. Part 3, Salicaceae – Cruciferae*. Berlings, Arlöv.

Borzenkova, I., Zorita, E., Borisova, O., Kalniņa, L., Kisielienė, D., Koff, T. et al. 2015. Climate change during the Holocene (past 12,000 years). In *Second Assessment of Climate Change for the Baltic Sea Basin*. Springer, Cham.

Blaauw, M. 2018. *rbacon. GitHub repository: GitHub*. Retrieved from https://github.com/cran/rbacon/commit/d90db914c28fa42772f1110bf7b990a7f94fa868 (accessed 2022-11-26).

Blaauw, M., Christen, J. A. and Lopez, M. A. A. 2021. *rbacon: Age-Depth modelling using Bayesian statistics*. https://cran.r-project.org/web/packages/rbacon/index.html (accessed 2022-11-26).

Blažauskas, N., Jurgaitis, A. and Šinkūnas, P. 2007. Patterns of Late Pleistocene proglacial fluvial sedimentation in the SE Lithuanian Plain. *Sedimentary Geology*, **193**(1–4), 193–201.

Blott, S. J. and Pye, K. 2001. GRADISTAT: a grain size distribution and statistics package for the analysis of unconsolidated sediments. *Earth Surface Processes and Landforms*, **26**(11), 1237–1248.

Bond, G., Showers, W., Cheseby, M., Lotti, R., Almasi, P., DeMenocal, P. et al. 1997. A pervasive millennial-scale cycle in North Atlantic Holocene and glacial climates. *Science*, **278**(5341), 1257–1266.

Bond, G., Kromer, B., Beer, J., Muscheler, R., Evans, M. N., Showers, W. et al. 2001. Persistent solar influence on North Atlantic climate during the Holocene. *Science*, **294**(5549), 2130–2136.

Broecker, W. S., Denton, G. H., Edwards, R. L., Cheng, H., Alley, R. B. and Putnam, A. E. 2010. Putting the Younger Dryas cold event into context. *Quaternary Science Reviews*, **29**(9), 1078–1081.

Cappers, R. T. J., Bekker, R. M. and Jans, J. E. A. 2006. *Digital Seed Atlas of the Netherlands*. Barkhuis Publishing & Groningen University Library, Groningen.

Catuneanu, O. 2006. *Principles of Sequence Stratigraphy*. Elsevier, Amsterdam.

Clemmensen, L. B., Pye, K., Murray, A. and Heinemeier, J. 2001. Sedimentology, stratigraphy and landscape evolution of a Holocene coastal dune system, Lodbjerg, NW Jutland, Denmark. *Sedimentology*, **48**, 3–27.

Conwy Valley Systems Limited. *PETROG. Trask Sorting*. Retrieved from https://ws2.petrog.com/articles/trask.html (accessed 2022-06-16).

Cuffey, K. M. and Clow, G. D. 1997. Temperature, accumulation, and ice sheet elevation in central Greenland through the last deglacial transition. *Journal of Geophysical Research: Oceans*, **102**(C12), 26383–26396.

Daumantas, L., Balakauskas, L. and Spiridonov, A. 2020. Machine learning reveals the role of the landscape in the dynamics of human settlement rules between the Palaeolithic and Iron Ages in Lithuania. *Quaternary International*, **565**, 109–124.

Donges, J. F., Donner, R. V., Marwan, N., Breitenbach, S. F. M., Rehfeld, K. and Kurths, J. 2015. Non-linear regime shifts in

Holocene Asian monsoon variability: potential impacts on cultural change and migratory patterns. *Climate of the Past*, **11**(5), 709–741.

Druzhinina, O., Kublitskiy, J., Stančikaitė, M., Nazarova, L., Syrykh, L., Gedminienė, L. et al. 2020. The Late Pleistocene–Early Holocene palaeoenvironmental evolution in the SE Baltic region: a new approach based on chironomid, geochemical and isotopic data from Kamyshovoye Lake, Russia. *Boreas*, **49**, 544–561.

Easterbrook, D. J. 2016. Temperature fluctuations in Greenland and the Arctic. In *Evidence-Based Climate Science*. 2nd ed. (Easterbrook, D. J. ed.). Elsevier, 137–160.

Gaglioti, B. V., Mann, D. H., Groves, P., Kunz, M. L., Farquharson, L. M., Reanier, R. E. et al. 2018. Aeolian stratigraphy describes ice-age paleoenvironments in unglaciated Arctic Alaska. *Quaternary Science Reviews*, **182**, 175–190.

Grigas, A. 1986. *Lietuvos augalų vaisiai ir sėklos* (*Fruits and seeds of Lithuanian plants*). Mokslas, Vilnius (in Lithuanian).

Grimm, E. C. 2007. *Tilia Version 1.0.1*. Illinois State Museum, Research and Collections Center, Springfield, IL.

Guobytė, R. and Satkūnas, J. 2011. Pleistocene glaciations in Lithuania. In *Quaternary Glaciations – Extent and Chronology. A Closer Look. Developments in Quaternary Science* (Ehlers, J., Gibbard, P. L. and Hughes, P. D., eds). Elsevier, Amsterdam, **15**, 231–246.

Haslett, J. and Parnell, A. C. 2008. A simple monotone process with application to radiocarbon-dated depth chronologies. *Journal of the Royal Statistical Society. Series C: Applied Statistics*, **57**(4), 399–418.

Ivanovic, R. F., Gregoire, L. J., Wickert, A. D., Valdes, P. J. and Burke, A. 2017. Collapse of the North American ice saddle 14,500 years ago caused widespread cooling and reduced ocean overturning circulation. *Geophysical Research Letters*, **44**(1), 383–392.

Kabailienė, M., Vaikutienė, G., Damušytė, A. and Rudnickaitė, E. 2009. Post–Glacial stratigraphy and palaeoenvironment of the northern part of the Curonian Spit, Western Lithuania. *Quaternary International*, **207**, 69–79.

Kalińska-Nartiša, E., Thiel, C., Nartišs, M., Buylaert, J.-P. and Murray, A. S. 2015. Age and sedimentary record of inland eolian sediments in Lithuania, NE European Sand Belt. *Quaternary Research*, **84**(1), 82–95.

Kasse, C. 2002. Sandy aeolian deposits and environments and their relation to climate during the Last Glacial Maximum and Lateglacial in northwest and central Europe. *Progress in Physical Geography*, **26**, 507–532.

Keigwin, L. D., Jones, G. A., Lehman, S. J. and Boyle, E. A. 1991. Deglacial meltwater discharge, North Atlantic deep circulation, and abrupt climate change. *Journal of Geophysical Research: Oceans*, **96**(C-9), 16811–16826.

Koch, P. L. and Barnosky, A. D. 2006. Late Quaternary extinctions: state of the debate. *Annual Review of Ecology, Evolution, and Systematics*, **37**, 215–250.

Łapcik, P., Ninard, K. and Uchman, A. 2021. Extra-large grains in Late Glacial–Early Holocene aeolian inland dune deposits of cold climate, European Sand Belt, Poland: an evidence of hurricane-speed frontal winds. *Sedimentary Geology*, **415**, 105847.

Liaw, A. and Wiener, M. 2002. Classification and regression by randomForest. *R News*, **2**(3), 18–22.

Loehle, C. and Singer, S. F. 2010. Holocene temperature records show millennial-scale periodicity. *Canadian Journal of Earth Sciences*, **47**(10), 1327–1336.

Lungershausen, U., Larsen, A., Bork, H.-R. and Duttmann, R. 2018. Anthropogenic influence on rates of aeolian dune activity within the northern European Sand Belt and socio-economic feedbacks over the last ~2500 years. *The Holocene*, **28**(1), 84–103.

Marcott, S. A., Shakun, J. D., Clark, P. U. and Mix, A. C. 2013. A reconstruction of regional and global temperature for the past 11,300 years. *Science*, **339**(6124), 1198–1201.

Matthews, J. A. and Seppälä, M. 2014. Holocene environmental change in subarctic aeolian dune fields: The chronology of sand dune re-activation events in relation to forest fires, palaeosol development and climatic variations in Finnish Lapland. *The Holocene*, **24**(2), 149–164.

Miall, A. D. 2010. *The Geology of Stratigraphic Sequences*. 2nd ed. Springer, Berlin, Heidelberg.

Molodkov, A. and Bitinas, A. 2006. Sedimentary record and luminescence chronology of the Lateglacial and Holocene aeolian sediments in Lithuania. *Boreas*, **35**, 244–254.

Norris, S., Garcia-Castellanos, D., Jansen, J. D., Carling, P. A., Margold, M., Woywitka, R. J. and Froese, D. G. 2021. Catastrophic drainage from the northwestern outlet of glacial Lake Agassiz during the Younger Dryas. *Geophysical Research Letters*, **48**(15), e2021GL093919.

Pierik, H. J., van Lanen, R. J., Gouw-Bouman, M. T., Groenewoudt, B. J., Wallinga, J. and Hoek, W. Z. 2018. Controls on late-Holocene drift-sand dynamics: the dominant role of human pressure in the Netherlands. *The Holocene*, **28**(9), 1361–1381.

Rasmussen, S. O., Bigler, M., Blockley, S. P., Blunier, T., Buchardt, S. L., Clausen, H. B. et al. 2014. A stratigraphic framework for abrupt climatic changes during the Last Glacial period based on three synchronized Greenland ice-core records: refining and extending the INTIMATE event stratigraphy. *Quaternary Science Reviews*, **106**, 14–28.

Rudnickaite, E. 1980. Методика определения карбонатов в разновозрастных моренах плейстоцена (The technique of the determination of carbonates in various age Pleistocene tills). In *Полевые и лабораторные методы исследования ледниковых отложений. Тезисы докладов межведомственного совещания* (*Methods of the field and laboratory investigations of glacial deposits. Abstracts of the symposium*). Academy of Sciences of the Estonian SSR, Tallinn, 121 (in Russian)

Rudnickaitė, E. 2007. Reconstruction of palaeogeography of Pleistocene interglacials according carbonates content. In *Proceedings of the XVII INQUA Congress "The Tropics: Heat Engine of the Quaternary", Cairns, Australia, 27 July–3 August 2007*. Abstracts / Quaternary International, **167–168**, Suppl. 356.

Rudnickaitė, E. 2016. *Carbonates in the Lithuanian Quaternary sediments as lithostratigraphic criterion and indicator of palaeoclimatic conditions*. Summary of doctoral dissertation. Vilnius University, Vilnius.

Sanko, A., Gaigalas, A.-J., Rudnickaitė, E. and Melešytė, M. 2008. Holocene malacofauna in calcareous deposits of Dūkšta site near Maišiagala in Lithuania. *Geologija*, **50**(4), 290–298.

Shao, Y. and Lu, H. 2000. A simple expression for wind erosion threshold friction velocity. *Journal of Geophysical Research: Atmospheres*, **105**, 22437–22443.

Spiridonov, A., Balakauskas, L., Stankevič, R., Kluczynska, G., Gedminienė, L. and Stančikaitė, M. 2019. Holocene vegetation patterns in southern Lithuania indicate astronomical forcing on the millennial and centennial time scales. *Scientific Reports*, **9**, 14711.

Spiridonov, A., Vaikutienė, G., Stankevič, R., Druzhinina, O., Šeirienė, V., Subetto, D. et al. 2021. Response of freshwater diatoms to cold events in the Late Pleistocene and Early Holocene (SE Baltic region). *Quaternary International*, **589**, 112–123.

Stančikaitė, M., Gedminienė, L., Edvardsson, J., Stoffel, M., Corona, C., Gryguc, G. et al. 2019. Holocene vegetation and hydroclimatic dynamics in SE Lithuania – Implications from a multi-proxy study of the Čepkeliai bog. *Quaternary International*, **501**(A), 219–239.

Stančikaitė, M., Kisielienė, D., Moe, D. and Vaikutienė, G. 2009. Lateglacial and early Holocene environmental changes in north-eastern Lithuania. *Quaternary International*, **207**(1–2), 80–92.

Snowball, I., Korhola, A., Briffa, K. R. and Koç, N. 2004. Holocene climate dynamics in Fennoscandia and the North Atlantic. In *Past Climate Variability through Europe and Africa. Developments in Paleoenvironmental Research, Vol. 6* (Battarbee, R. W., Gasse, F. and Stickley, C. E., eds). Springer, Dordrecht, 465–494.

Teller, J. T., Leverington, D. W. and Mann, J. D. 2002. Freshwater outbursts to the oceans from glacial Lake Agassiz and their role in climate change during the last deglaciation. *Quaternary Science Reviews*, **21**(8–9), 879–887.

Tolksdorf, J. F. and Kaiser, K. 2012. Holocene aeolian dynamics in the European sand-belt as indicated by geochronological data. *Boreas*, **41**(3), 408–421.

Veski, S., Seppä, H. and Ojala, A. E. K. 2004. Cold event at 8200 yr B.P. recorded in annually laminated lake sediments in eastern Europe. *Geology*, **32**(8), 681–684.

Veski, S., Seppä, H., Stančikaitė, M., Zernitskaya, V., Reitalu, T., Gryguc, G. et al. 2015. Quantitative summer and winter temperature reconstructions from pollen and chironomid data between 15 and 8 ka BP in the Baltic–Belarus area. *Quaternary International*, **388**, 4–11.

White, D., Preece, R. C., Shchetnikov, A. A. and Dlussky, K. G. 2013. Late Glacial and Holocene environmental change reconstructed from floodplain and aeolian sediments near Burdukovo, lower Selenga River Valley (Lake Baikal region), Siberia. *Quaternary International*, **290–291**, 68–81.

Wolbach, W. S., Ballard, J. P., Mayewski, P. A., Parnell, A. C., Cahill, N., Adedeji, V. et al. 2018. Extraordinary biomass-burning episode and impact winter triggered by the Younger Dryas cosmic impact ~12,800 years ago. 2. Lake, marine, and terrestrial sediments. *The Journal of Geology*, **126**(2), 185–205.

Woronko, B., Zieliński, P. and Sokołowski, R. J. 2015. Climate evolution during the Pleniglacial and Late Glacial as recorded in quartz grain morphoscopy of fluvial to aeolian successions of the European Sand Belt. *Geologos*, **21**(2), 89–103.

Xu, Z., Stevens, T., Yi, S., Mason, J. A. and Lu, H. 2018. Seesaw pattern in dust accumulation on the Chinese Loess Plateau forced by late glacial shifts in the East Asian monsoon. *Geology*, **46**(10), 871–874.

Zeeberg, J. 1998. The European sand belt in Eastern Europe and comparison of Late Glacial dune orientation with GCM simulation results. *Boreas*, **27**(2), 127–139.

Zervynose paleojärve settimistingimused ja karbonaatide sisaldus hilisjääajast Kesk-Holotseenini.

Liudas Daumantas, Petras Šinkūnas, Eugenija Rudnickaitė, Nikita Dobrotin, Dalia Kisielienė ja Andrej Spiridonov

Artikkel käsitleb Euroopa hilisjääaegses nn liivavööndis (European Sand Belt) asuvat Zervynos-2 paleojärve setteläbilõiget (Kagu-Leedu) luidete ja paleosetete vaheldumise aspektist. Settimiskeskkonda iseloomustatakse granulomeetriliste parameetrite, setete struktuuriomaduste, dolomiidi/kaltsiidi suhte ja taimsete suurjäänuste analüüsi kaudu. Uuring näitas, et Zervynos-2 järv tekkis kohe pärast jääliustiku taganemist sanduri tasandikul. Analüüsitud järvemuda karbonaatide suhe ja taimejäänused näitasid kliimamuutuste mõningast ebasünkroonsust Grööonimaa jääandmetega. Üleminek liiva settimisele paleojärves algas ligikaudu Holotseeni keskpaigas, mis seostub kliima soojenemise ja vähese niiskusega. Paleojärve hilisem areng on eoolset päritolu ning settimine on aeglane.